



OPEN

Temporal dynamics from phosphoproteomics using endoscopic biopsy specimens provides new therapeutic targets in stage IV gastric cancer

Hidekazu Hirano^{1,2,3,4}, Yuichi Abe^{1,2,13}, Yosui Nojima^{7,8}, Masahiko Aoki^{3,11}, Hirokazu Shoji³, Junko Ioyama^{1,2}, Kazufumi Honda^{5,6}, Narikazu Boku^{3,12}, Kenji Mizuguchi^{7,9}, Takeshi Tomonaga^{1,2}✉ & Jun Adachi^{1,2,10}✉

Phosphoproteomic analysis expands our understanding of cancer biology. However, the feasibility of phosphoproteomic analysis using endoscopically collected tumor samples, especially with regards to dynamic changes upon drug treatment, remains unknown in stage IV gastric cancer. Here, we conducted a phosphoproteomic analysis using paired endoscopic biopsy specimens of pre- and post-treatment tumors (Ts) and non-tumor adjacent tissues (NATs) obtained from 4 HER2-positive gastric cancer patients who received trastuzumab-based treatment and from pre-treatment Ts and NATs of 4 HER2-negative gastric cancer patients. Our analysis identified 14,622 class 1 phosphosites with 12,749 quantified phosphosites and revealed molecular changes by HER2 positivity and treatment. An inhibitory signature of the ErbB signaling was observed in the post-treatment HER2-positive T group compared with the pre-treatment HER2-positive T group. Phosphoproteomic profiles obtained by a case-by-case review using paired pre- and post-treatment HER2-positive T could be utilized to discover predictive or resistant biomarkers. Furthermore, these data nominated therapeutic kinase targets which were exclusively activated in the patient unresponsive to the treatment. The present study suggests that a phosphoproteomic analysis of endoscopic biopsy specimens provides information on dynamic molecular changes which can individually characterize biologic features upon drug treatment and identify therapeutic targets in stage IV gastric cancer.

Gastric cancer is the third leading cause of cancer-related death worldwide¹. Over the past two decades, the therapeutic landscape for advanced gastric cancer has changed significantly with the approval of new agents. Trastuzumab and trastuzumab deruxtecan used as the standard-of-care in human epidermal growth factor

¹Laboratory of Proteome Research, National Institute of Biomedical Innovation, Health and Nutrition, Osaka 567-0085, Japan. ²Laboratory of Proteomics for Drug Discovery, Center for Drug Design Research, National Institute of Biomedical Innovation, Health and Nutrition, Osaka 567-0085, Japan. ³Gastrointestinal Medical Oncology Division, National Cancer Center Hospital, Tokyo 104-0045, Japan. ⁴Department of Medicine, Keio University Graduate School of Medicine, Tokyo 160-8582, Japan. ⁵Department of Biomarkers for Early Detection of Cancer, National Cancer Center Research Institute, Tokyo 104-0045, Japan. ⁶Department of Bioregulation, Nippon Medical School, Bunkyo-ku, Tokyo 113-8602, Japan. ⁷Laboratory of Bioinformatics, Artificial Intelligence Center for Health and Biomedical Research (ArCHER), National Institutes of Biomedical Innovation, Health and Nutrition, Osaka 567-0085, Japan. ⁸Center for Mathematical Modeling and Data Science, Osaka University, Osaka 560-8531, Japan. ⁹Institute for Protein Research, Osaka University, Osaka 565-0871, Japan. ¹⁰Laboratory of Clinical and Analytical Chemistry, Center for Drug Design Research, National Institute of Biomedical Innovation, Health and Nutrition, Osaka 567-0085, Japan. ¹¹Kyoto Innovation Center for Next Generation Clinical Trials and iPSC Cell Therapy (Ki-CONNECT), Kyoto University Hospital, Kyoto 606-8507, Japan. ¹²Department of Medical Oncology and General Medicine, IMSUT Hospital, Institute of Medical Science, University of Tokyo, Tokyo 108-8639, Japan. ¹³Division of Molecular Diagnostics, Aichi Cancer Center Research Institute, Nagoya 464-8681, Japan. ✉email: tomonaga@nibiohn.go.jp; jun_adachi@nibiohn.go.jp

receptor 2 (HER2)-positive gastric cancer, which accounts for 20% of all gastric cancers^{2,3}. Based on the results of phase 3 trials, fluoropyrimidine plus platinum with or without nivolumab (immune checkpoint inhibitor) is the standard-of-care for HER2-negative advanced gastric cancer in the first-line setting and fluoropyrimidine plus platinum with trastuzumab for HER2-positive advanced gastric cancer^{2,4,5}. However, the majority of patients experience disease progression during the treatment and there remains an unmet need for more effective therapeutic options for advanced gastric cancer.

The facilitation of large-scale genomic research following the advent of next generation sequencing has provided insights into the biology of gastric cancer^{6,7}. Concurrently, comprehensive genomic profiling has been implemented for personalization of therapeutic options in clinical practice. Despite the introduction of precision medicine, only a small fraction of patients has received genomically-matched treatments^{8,9}. In gastric cancer, the scarcity of targetable genetic alterations is an important feature¹⁰. Therefore, new approaches for identifying biological features beyond genomic characterization are required to make additional breakthroughs in personalized medicine. In this regard, correlating proteomic profiles with specific cancer phenotypes has the potential to expand the therapeutic horizon in advanced gastric cancer.

Phosphorylation is one of the most common posttranslational modifications and regulates many biological processes including oncogenesis. The Clinical Proteomic Tumor Analysis Consortium performed proteomic/phosphoproteomic characterization of multiple types of solid tumors, and proposed that phosphoproteomic analysis could be used to identify therapeutic targets^{11–19}. In addition, high-sensitive phosphoproteomic analyses have been performed using cancer cell lines and surgical specimens^{20,21}. For patients with metastatic cancer treated with drug therapy, it is required to obtain tumor tissues for application of phosphoproteomic analysis on demand (e.g., at disease progression), which limits the type of clinical specimens. It is highly invasive to perform surgical resection of tumors with the intent for tissue collection in patients with stage IV gastric cancer. Furthermore, phosphoproteomic status changes rapidly and can be affected by ischemia during surgical procedures²². These issues hamper the clinical applicability of phosphoproteomic analysis in patients with metastatic disease. To overcome this problem, we have developed a highly sensitive phosphoproteomic analysis platform using fresh-frozen endoscopic biopsy specimens containing a small amount of protein (approximately 300 µg/specimen)²³. Using this platform, we performed kinase-substrate enrichment analysis of phosphoproteomic data using paired gastric cancer tissues and normal gastric tissues at static condition and found that cell cycle-related kinases and DNA damage response signals were activated in the cancer. Furthermore, the kinase activity profiles of tumors differed greatly among individuals.

Although molecular targeted agents can elicit an impressive initial response, intrinsic and acquired drug resistance is a relevant problem, dampening long-term disease control. Serial biopsies after administration of molecular targeted agents can reveal changes in activation or inhibition of intracellular signaling pathways, thereby helping to identify resistance mechanisms in individual patients. In this context, phosphoproteomic analysis of serial endoscopic biopsy specimens during treatment or upon progression, may facilitate the elucidation of resistance mechanisms and the discovery of therapeutic targets. However, the feasibility and molecular significance of phosphoproteomic analysis using tumor specimens collected sequentially remain unknown.

Here, we conducted a phosphoproteomic analysis using endoscopic biopsy specimens obtained from stage IV gastric cancer patients. Especially, we investigated the dynamic molecular changes after trastuzumab-containing therapy in HER2-positive gastric cancer using paired pre- and post-treatment tumor specimens for evaluating the utility of our method to understand the effect of drug therapy involving a molecular targeted agent from the phosphoproteomic landscape. In addition, we estimated the spectrum of active kinase of gastric cancer by comparing tumor specimens with non-tumor adjacent tissues on a case-by-case basis.

Results

Overview of phosphoproteomic analysis. Figure 1 shows a schematic diagram of quantitative phosphoproteomic analysis of gastric tumor tissues (Ts) and non-tumor adjacent tissues (NATs) before and after trastuzumab-based treatment of four patients with HER2-positive cancer and Ts and NATs from four patients with HER2-negative cancer (Fig. S1a).

Clinical information on the patients is summarized in Table 1. With the exception of Patient 4, a partial response (PR) was elicited by drug therapy in all patients with HER2-positive gastric cancer. In total, 14,622 class 1 phosphosites including 12,059 phospho-serine sites (82.5%), 2,307 phospho-threonine sites (15.8%), and 256 phospho-tyrosine sites (1.8%) were identified from the phosphoproteomic data (Fig. 2a,b). Of the class 1 phosphosites, 12,749 phosphosites (87.2%) had quantitative values in at least one sample (Fig. 2a). Of the quantified phosphosites, the percentage of phosphosites that showed quantitative values in all three groups (cell line mixture, primary tumor tissue, and non-tumor adjacent tissue) was 97.6% and the percentage that showed quantitative values only in the cell line mixture samples was 0.6% (Fig. S1b). In total, 4,986 proteins were identified from global proteomic analysis. Of quantified protein in at least one sample (4,809 proteins), the percentage of proteins that showed quantitative values in all three groups (cell line mixture, primary tumor tissue, and non-tumor adjacent tissue) was 99.7% and the percentage that showed quantitative values only in the cell line mixture samples was 0% (Fig. S1c).

Next, we performed principal component analysis (PCA) using batch-corrected phosphoproteomic and proteomic data (data without batch correction: Table S1 [phosphoproteomic analysis], S2 [global proteomic analysis]; data with batch correction: Table S3 [phosphoproteomic analysis], Table S4 [global proteomic analysis]). PCA using phosphoproteomic data revealed a clear separation between HER2-negative T and pre-treatment HER2-positive T (Fig. 2c). In addition, plots of post-treatment HER2-positive T were completely shifted from those of pre-treatment HER2-positive T (Fig. 2c). Taken together, these results indicate that HER2 positivity and drug treatment have clear effects on the phosphoproteomic signature. Plots of NAT samples before and

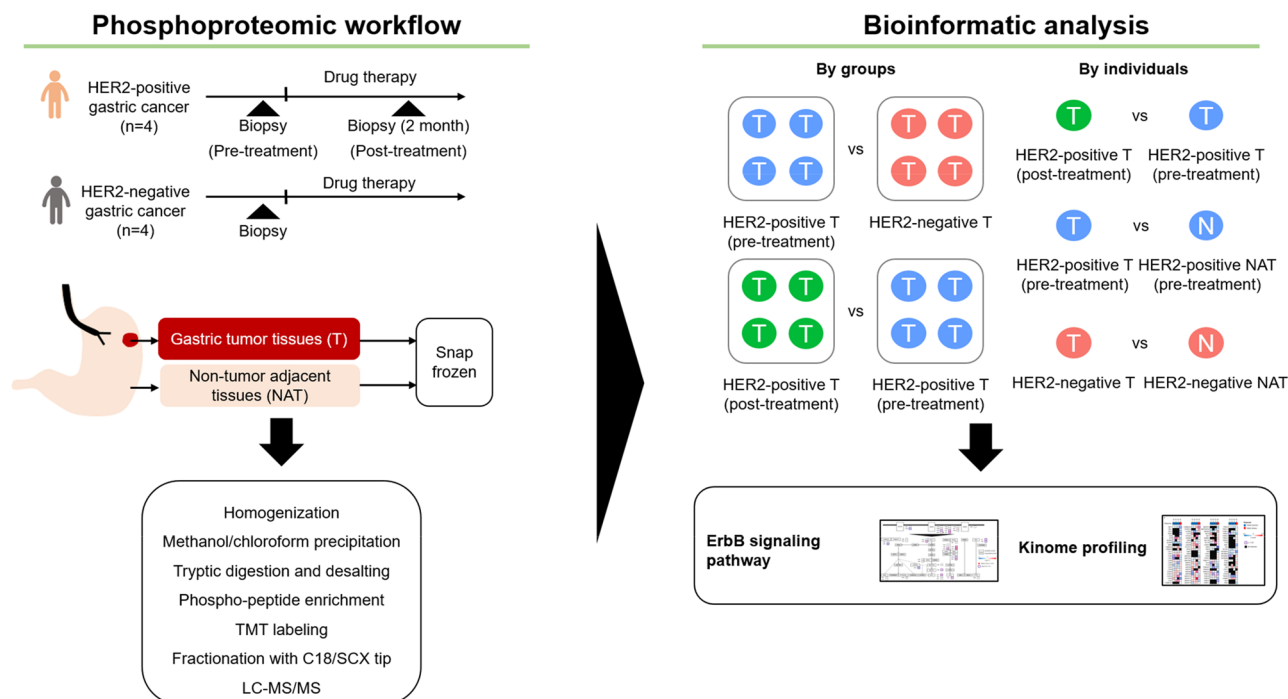


Figure 1. Schematic diagram of the quantitative phosphoproteomic analysis in this study. Using endoscopic procedures, tumor tissues and non-tumor adjacent tissues were collected from four patients with HER2-positive gastric cancer (before and after drug therapy [trastuzumab-containing therapy]) and four patients with HER2-negative gastric cancer. Those specimens were subject to sample preparation for quantitative phosphoproteomic analysis. Using phosphoproteomic data, bioinformatics analyses were conducted to evaluate molecular differences by groups and by individuals.

| Patient | Age | Sex | Metastatic site | Stage | Histology | Prior treatment | Treatment | BOR |
|-----------------|-----|--------|--------------------|-------|------------|-----------------|------------|-----|
| HER2-positive 1 | 59 | Male | LYM, HEP, PER | IV | Intestinal | None | SOX + Tmab | PR |
| HER2-positive 2 | 44 | Female | LYM, PER | IV | Diffuse | None | XP + Tmab | PR |
| HER2-positive 3 | 66 | Female | LYM, HEP | IV | Intestinal | None | XP + Tmab | PR |
| HER2-positive 4 | 64 | Male | LYM, HEP, PER, PUL | IV | Diffuse | None | XP + Tmab | SD |
| HER2-negative 1 | 72 | Male | LYM, HEP | IV | Intestinal | Yes | | |
| HER2-negative 2 | 68 | Male | LYM, HEP, PER | IV | Intestinal | None | | |
| HER2-negative 3 | 71 | Female | LYM, PER | IV | Diffuse | None | | |
| HER2-negative 4 | 64 | Female | LYM, PER, PLU | IV | Diffuse | None | | |

Table 1. Summary of clinical information on the patients for the phosphoproteomic analysis. Best overall response was defined according to the Response Evaluation Criteria in Solid Tumors (RECIST) version 1.1. BOR best overall response, HEP liver, HER2 human epidermal growth factor receptor 2, LYM lymph node, PER peritoneum, PLU pleura, PR partial response, PUL lung, SD stable disease, SOX S-1 plus oxaliplatin, Tmab trastuzumab, XP capecitabine plus cisplatin.

after drug treatment were overlapped, indicating that drug treatment had less of an effect on the NAT phosphoproteomic profiles (Fig. 2d). PCA using global proteomic data from T or NAT samples suggested that the phosphoproteomic data separated tumors more clearly according to HER2 positivity and treatment exposure (Fig. S2a,b). Although the differences were not statistically significant, HER2 expression tended to be higher in the pre-treatment HER2-positive T group compared with the post-treatment HER2-positive T group, and with the HER2-negative T group (Fig. S2c).

Comparison of phosphorylation status between the pre-treatment HER2-positive and the HER2-negative T group. To capture unique phosphosites in HER2-positive gastric cancer, we overlaid the phosphoproteomic data from the pre-treatment HER2-positive and HER2-negative T groups with phosphosites in the ErbB signaling pathway in the Kyoto Encyclopedia of Genes and Genomes (KEGG) database (Fig. 3, Table S5). Several phosphosites in the ErbB signaling pathway were upregulated with significance (HER2 [T733]) or with a tendency (PAK2 [T143], MYC [S62]) in the HER2-positive T group. Of note, increased phos-

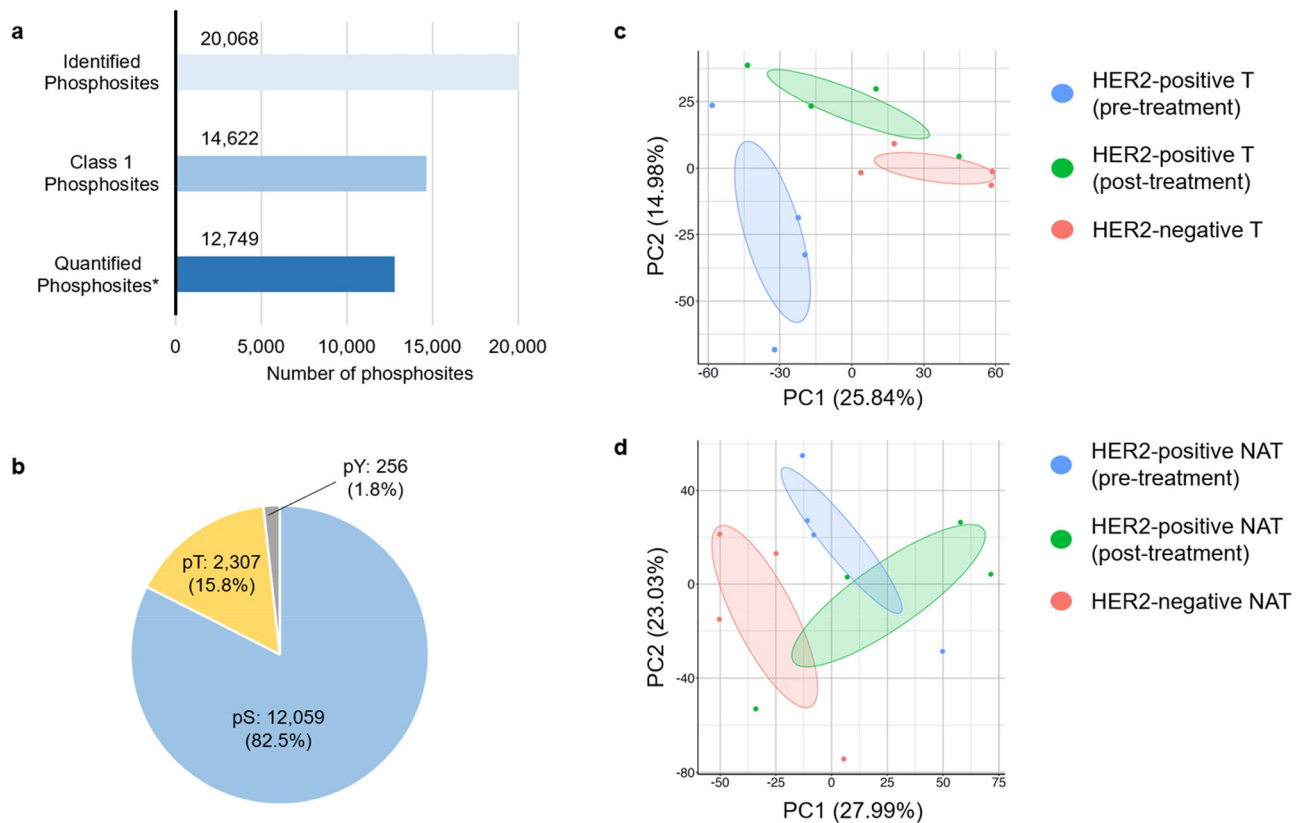


Figure 2. Summary of the results of phosphoproteomic analysis. **(a)** Number of identified phosphosites, class 1 phosphosites, quantified class 1 phosphosites. Asterisk (quantified phosphosites) means the phosphosites with quantitative values in at least one sample. **(b)** The proportions of phospho-serine (pS, blue), phospho-threonine (pT, yellow), phospho-tyrosine (pY, grey). **(c)** Principal component analysis of tumor samples using phosphoproteomic data. **(d)** Principal component analysis of non-tumor adjacent samples using phosphoproteomic data.

phorylation of serine 62 of MYC is indicative of the activation of this multifunctional oncoprotein, which cooperates with HER2 to stimulate cell proliferation^{24,25}. Increased phosphorylation of MAP2K2 (MEK2) at threonine 394 and MAPK1 (ERK2) at threonine 185 was observed without statistical significance or tendency, which might be associated with inhibition of negative feedback of RAS/ERK signaling, resulting in HER2 (Y1248) downregulation^{26,27}. These results suggest that the ErbB signaling is activated in HER2-positive gastric cancer compared with HER2-negative gastric cancer.

Then, we performed pathway enrichment analysis for differentially expressed phosphosites with significance between two groups (402 upregulated phosphosites in the pre-treatment HER2-positive T group and 478 upregulated phosphosites in the HER2-negative T group, as shown in Fig. S3a,b and Table S5). The results of pathway analysis with p -values < 0.05 are summarized in Table S5. Of note, the phosphosites upregulated in the HER2-positive T group were involved in lysine degradation, consistent with a previous finding by whole-genome sequencing²⁸. The phosphosites upregulated in the HER2-negative T group were involved in glycerophospholipid metabolism and the p53 signaling pathway.

Phosphoproteomic changes after drug therapy in HER2-positive gastric cancer. Next, we investigated the impact of drug therapy on the ErbB signaling pathway in the post-treatment HER2-positive T group versus the pre-treatment HER2-positive T group (Fig. 4, Table S6). An inhibitory signature of the ErbB signaling was observed without statistical significance or tendency in post-treatment HER2-positive T group, such as the downregulation of mTOR (RPS6KB2 [S6K2, (S423)]), and JUN signaling (PAK1 [T212], PAK2 [S141], JUN [S73]). Decreased levels of these phosphosites are associated with inactivation of the corresponding oncoproteins^{29–36}. In addition, the decreased phosphorylation of MAP2K2 (MEK2) at threonine 394 and MAPK1 (ERK2) at threonine 185 might be explained by the inhibition of the ErbB signaling by drug therapy^{26,27}. HER2 (S1054) and MYC (T58) tended to be upregulated in the post-treatment HER2-positive T group. The increased phosphorylation of the serine 1054 residue of HER2 might be due to a feedback response to anti-HER2 blockade²⁶. In addition, phosphorylation of MYC at threonine 58 results in proteasomal degradation of this oncoprotein³⁷. Collectively, these data capture inhibitory modifications of the ErbB signaling pathway in post-treatment HER2-positive gastric cancer.

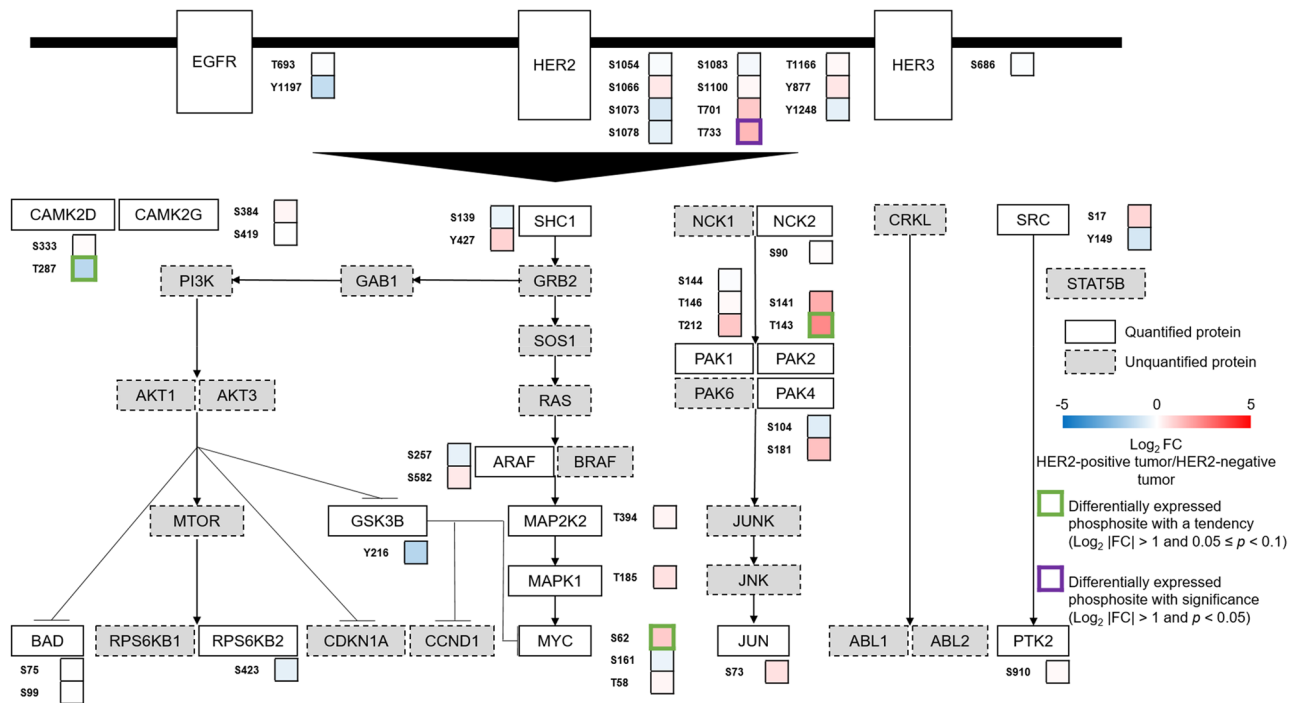


Figure 3. Dynamics of phosphosites in the ErbB pathway (the HER2-positive gastric cancer [pre-treatment] group versus the HER2-negative gastric cancer group). Proteins in the ErbB signaling pathway are selected from the KEGG database⁶⁵. Proteins with quantified phosphosites are shown as white boxes with solid lines. Proteins without quantified phosphosites are shown as grey boxes with dotted lines. Differentially expressed phosphosites with significance ($\log_2 |FC| > 1$ and $p < 0.05$) are depicted by a purple line. Differentially expressed phosphosites with a tendency ($\log_2 |FC| > 1$ and $0.05 \leq p < 0.1$) are depicted by a green line.

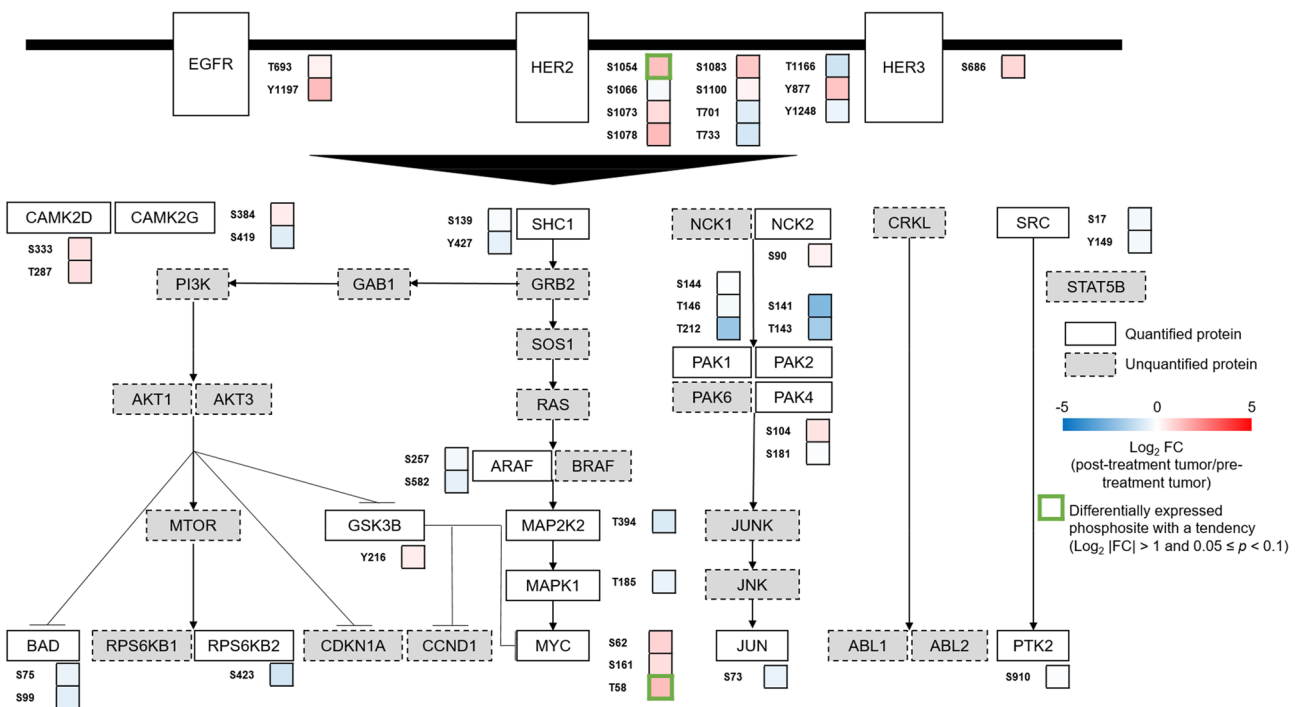


Figure 4. Dynamics of phosphosites in the ErbB pathway (between pre- and post-treatment the HER2-positive gastric cancer groups). Proteins in the ErbB signaling pathway are selected from the KEGG database⁶⁵. Proteins with quantified phosphosites are shown as white boxes with solid lines. Proteins without quantified phosphosites are shown as grey boxes with dotted lines. Differentially expressed phosphosites with a tendency ($\log_2 |FC| > 1$ and $0.05 \leq p < 0.1$) are depicted by a green line.

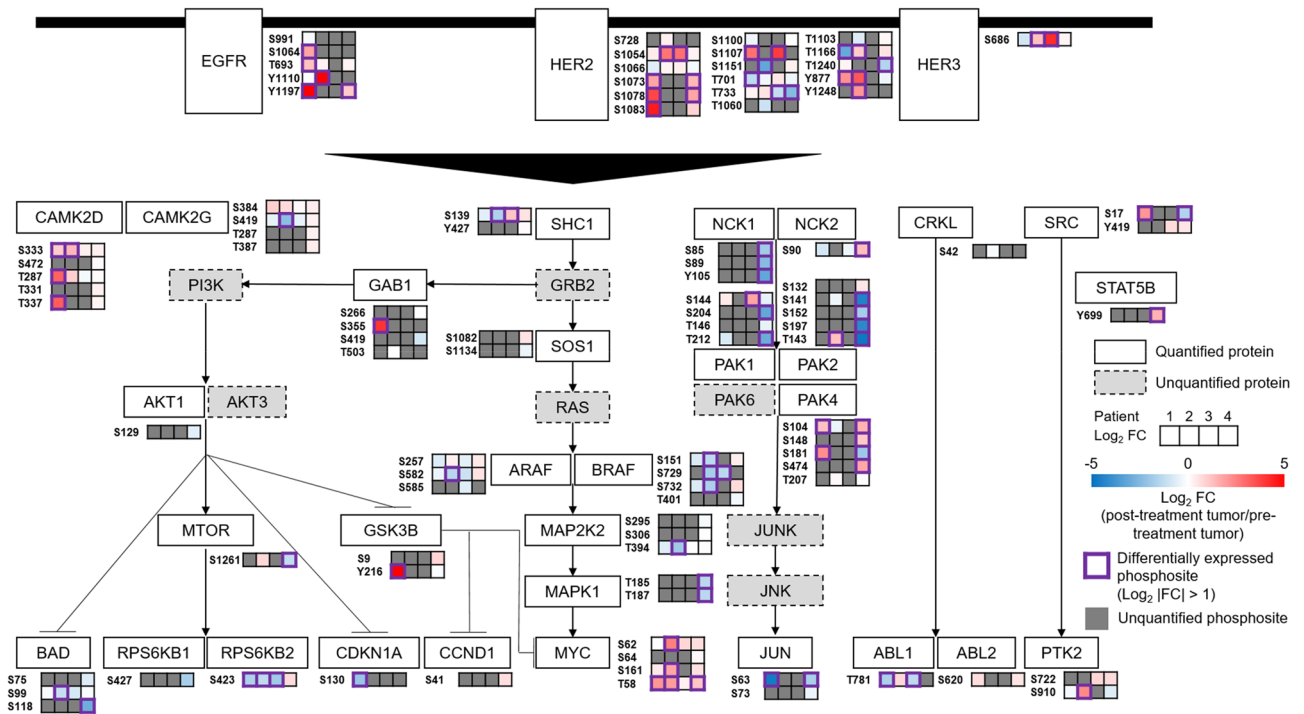


Figure 5. Individual comparison of phosphorylation status between pre- and post-treatment HER2-positive gastric cancer. Proteins in the ErbB signaling pathway are selected from the KEGG database⁶⁵. Proteins with quantified phosphosites are shown as white boxes with solid lines. Proteins without quantified phosphosites are shown as grey boxes with dotted lines. Differentially expressed phosphosites ($\log_2 |FC| > 1$) are depicted by a purple line. Phosphosites with no quantitative value are filled with grey.

Then, we performed pathway enrichment analysis for differentially expressed phosphosites with significance between two groups. (209 upregulated phosphosites and 135 downregulated phosphosites in the post-treatment HER2-positive T group, as shown in Fig. S4a,b and Table S6). The results of pathway analysis with p -values < 0.05 are summarized in Table S6. The spliceosome pathway was included among the increased activated pathways in the post-treatment HER2-positive group. Spliceosomes play a role in the alternative mRNA splicing machinery, which is induced by platinum and trastuzumab-based treatment^{38,39}. In addition, the nucleotide excision repair pathway was also activated. Nucleotide excision repair is an important cellular defense mechanism against platinum agents that elicit DNA damage⁴⁰. Taken together, these data suggest that our method provides information on phosphoproteomic changes associated with the response to drug therapy in HER2-positive gastric cancer.

Individual variation of phosphorylation status in ErbB signaling after drug therapy in HER2-positive gastric cancer.

We assumed that individual phosphoproteomic data might show inter-patient variations. To capture individual variation of phosphorylation status in the ErbB signaling upon drug therapy, a case-by-case review using paired pre- and post-treatment HER2-positive T samples derived from 4 patients was performed (Fig. 5, Table S7). In this analysis, a total of 17 phosphosites on HER2 protein were quantified in at least one patient. Considering that the function of those phosphosites in tumor is largely unexplored, we focused on the downstream components of the ErbB pathway to investigate the effects anti-HER2 blockade⁴¹. Our data revealed that RPS6KB2 (S6K2, [S423]) and NCK2 (S90) phosphosites were upregulated only in Patient 4 (who did not experience a PR) but were downregulated in Patient 1–3 (each of whom experienced a PR). Notably, phosphorylation of serine 423 of RPS6KB2 (S6K2) leads to its activation, suggesting that this phosphosite is a predictive biomarker for the efficacy of trastuzumab-based treatment³⁵. In addition, we observed the upregulation of several other phosphosites in the post-treatment tumor of Patient 4, such as PAK4 (S474) and STAT5B (Y699), potentially associated with bypass mechanisms for acquired resistance^{42,43}. Among three patients who achieve a PR, complex variations in the activation were shown in the ErbB pathway. As a common feature, downregulation of several phosphosites on RAF proteins were observed exclusively in responded patients, suggesting an effect of HER2 blockade on the ErbB pathway⁴⁴. Collectively, these phosphoproteomic data reveal distinct profiles in signaling pathways on an individual patient level and could thus be used for identifying molecules that predict the response to drug therapy or link to acquired resistance.

Individual activated kinases after drug therapy for HER2-positive gastric cancer. Considering the clinical success in the development of kinase inhibitors, an understanding of kinome-wide dysregulation may help to individualize cancer treatment further. We subjected our individual phosphoproteomic data of HER2-positive gastric cancer to kinase-substrate enrichment analysis (KSEA) to identify active kinases after

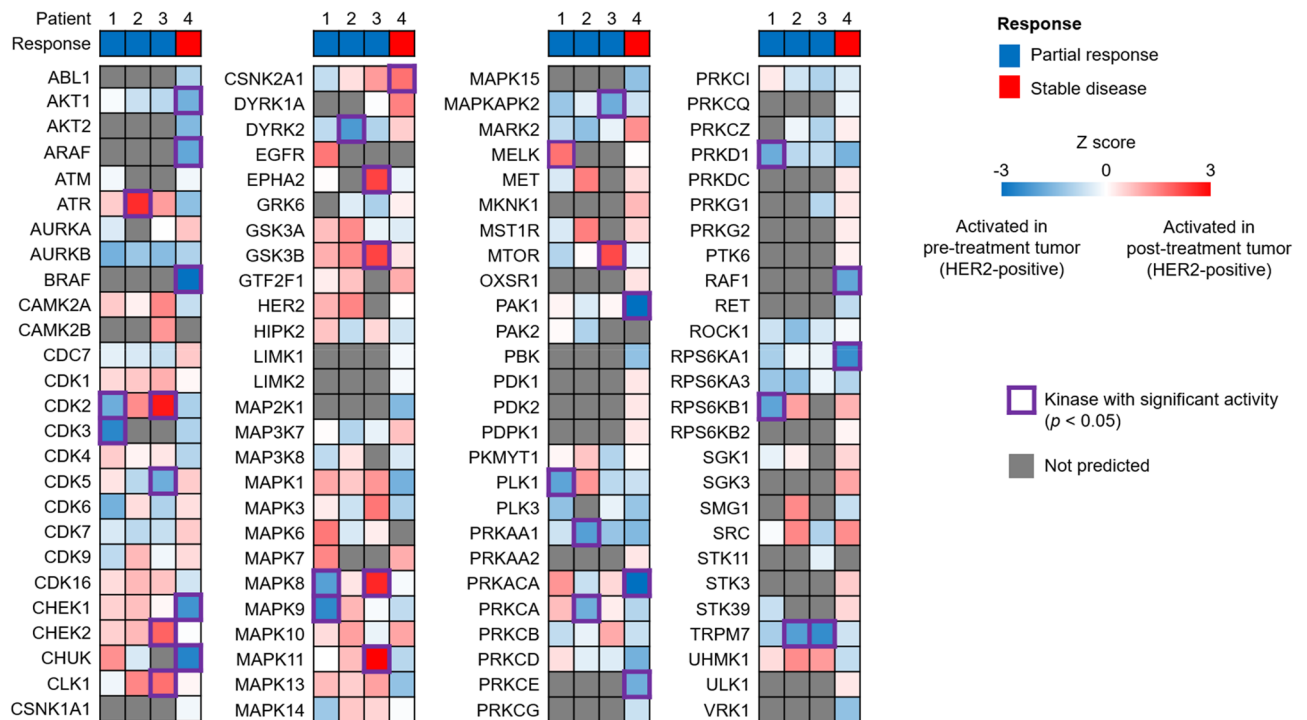


Figure 6. Individual kinome profiling of post-treatment HER2-positive gastric cancer in comparison with the corresponding pre-treatment HER2-positive gastric cancer. Information on the responses to drug therapy is shown at the top of the kinome profiling. Kinases with significant activity ($p < 0.05$) are depicted by purple lines. Kinases with no information are filled with grey.

drug therapy in a personalized manner (Fig. 6, Table S8). Patient-specific profiles showed no clear difference in kinase activities between responding and non-responding patients, suggesting that the change in kinase activities in response to drug therapy was highly inter-individual. Notably, several kinases were upregulated exclusively in Patient 4 in whom PR was not achieved, including AURKA, CDC7, CDK7, DYRK1A, MAP3K7, MARK2, RPS6KB2 (S6K2), SGK3, STK3, STK39, and ULK. Activation of these kinases might be associated with acquired resistance to drug therapy and they may be candidates for therapeutic targets. Phosphoproteomic data also revealed trends of upregulation of phosphorylation at sites that activate two kinases (CDK7[T170], RPS6KB2(S6K2) [S423]) after treatment in the post-treatment tumor of Patient 4 compared with those of the other patients (Fig. S5, Table S7). Taken together, these data suggest that phosphoproteomic analysis might be used to evaluate kinase activity after drug therapy and potentially guide therapeutic strategies on an individual patient level.

Individual activated kinases in T compared to NAT. Next, we exploited our analysis of individual phosphoproteomic data of T and NAT using KSEA to identify kinases that were activated in pre-treatment HER2-positive and HER2-negative gastric cancer (Fig. 7a,b, Table S9, S10). Regardless of HER2 positivity, kinases in cell cycle pathways (e.g., CDK2, CDK6) or those involved in the DNA damage response (e.g., ATM, ATR, CHEK2) were upregulated. Intriguingly, there was no signal of strong HER2 activation in pre-treatment HER2-positive gastric cancer samples, despite the increased HER2 protein level in this group (Fig. S2c), indicating the complexity of the relationship between protein abundance and functionality.

Discussion

In this study, we performed phosphoproteomic analysis of advanced gastric cancer using endoscopic biopsy specimens. By using endoscopic specimens immediately frozen in liquid nitrogen, we minimized the ischemic effect on protein phosphorylation for obtaining physiological phosphoproteomic data. Even with limited amount of protein, we identified more than 14,000 class 1 phosphosites, allowing characterization of tumor biology not only before but also after drug therapy in metastatic disease. Distinct differences in phosphorylation status were observed between HER2-positive cancer and HER2-negative cancer, and between pre- and post-treatment HER2-positive cancer. By coupling individual phosphoproteomic data with kinase-substrate relationships, activated kinases in post-treatment tumors in comparison with pre-treatment tumors with regards to HER2-positive gastric cancer, and those in tumors in comparison with non-tumor adjacent tissues could be inferred in a personalized manner. To our knowledge, the present study firstly demonstrated the concept of investigating the dynamic molecular changes induced by drug therapy from the phosphoproteomic landscape in stage IV gastric cancer.

By comparing the phosphoproteomic data of pre- and post-treatment HER2 positive gastric cancer groups, we detected an inhibitory signature of the ErbB signaling after trastuzumab-based treatment. In addition, pathway

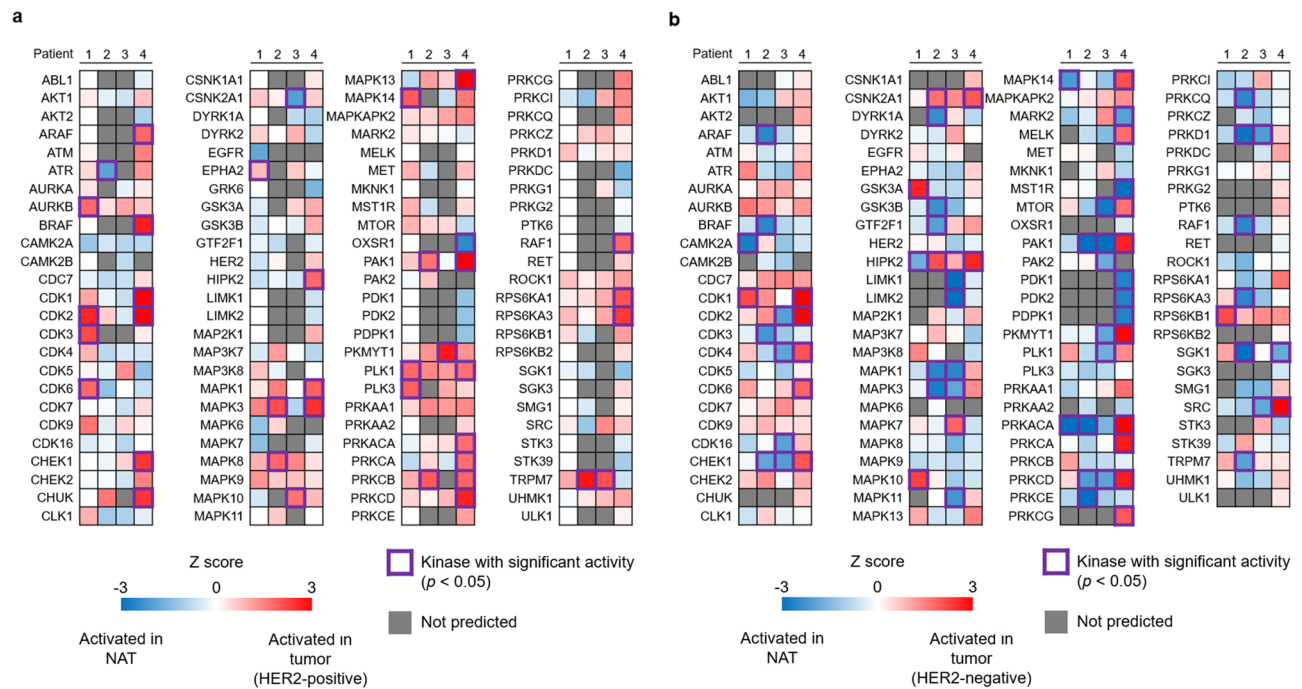


Figure 7. Individual kinome profiling of gastric cancer versus the corresponding non-tumor adjacent tissue. Information on the patients is shown at the top of the kinome profiling. Kinases with significant activity ($p < 0.05$) are depicted by purple lines. Kinases with no information are filled with grey. **(a)** Kinase profiles of pre-treatment HER2-positive gastric cancer. **(b)** Kinase profiles of HER2-negative gastric cancer.

enrichment analysis showed that particular pathways that were activated in specific groups (e.g., lysine degradation in pre-treatment HER2-positive gastric cancer compared with HER2-negative cancer; spliceosome and nucleotide excision repair pathways in the post-treatment HER2-positive gastric cancer compared with pre-treatment HER2-positive gastric cancer). A case-by-case review of comparison of pre- and post-phosphoproteomic data, a significant downregulation of RPS6KB2 (S6K2, [S423]) was observed in three patients with a PR but not in one patient with a PR. Previous researches revealed demonstrate that trastuzumab inhibits the phosphorylation of S6K^{45,46}. In addition, trastuzumab-based treatment requires the inhibition of S6K phosphorylation to enhance fluorouracil-induced apoptosis in gastric cancer cell lines with HER2 amplification⁴⁵. Considering that activation of RPS6KB2 (S6K2) is accompanied by phosphorylation of specific sites such as S423, our data indicate that the phosphorylation level of RPS6KB2 (S6K2, [S423]) immediately after administration of treatment can be utilized as a predictive marker for the response to trastuzumab-based treatment⁴⁷. Thus, phosphoproteomic data could be useful for exploring phosphosites that are informative for predicting anti-tumor efficacy before response evaluation in clinical practice.

Our workflow enabled us to explore molecular variations in response to drug therapy that might contribute to acquired resistance. For example, upregulation of STAT5B (Y699) was found exclusively in the patient whose tumor did not respond to therapy. The observation was consistent with a previous report demonstrating an association between STAT5 phosphorylation with the response to anti-HER therapy⁴⁸. We also found PAK4 (S474) hyperphosphorylation exclusively in the same patient. These phosphosites may play a role in acquired resistance to trastuzumab-based treatment via a bypass mechanism^{42,43}. In addition, our analysis identified kinases that were activated after drug therapy for HER2-positive gastric cancer. Of note, the kinases that were activated exclusively in the patient without a PR might be considered as potential molecules for overcoming treatment resistance (e.g., RPS6KB2 [S6K2], CDK7, STK3, and STK39). RPS6KB2 (S6K2) and CDK7 activation were supported by phosphoproteomic data which revealed upregulation of phosphorylation at sites which mediate these kinases. CDK7 inhibitors have been under investigation in clinical trials⁴⁹. CDK7 overexpression is associated with poor survival in patients with gastric cancer, whereas CDK7 inhibition decreases the proliferation in a gastric cancer cell line, suggesting CDK7 as a potential therapeutic target⁵⁰. Of note, STK3 and STK39 activation were reported in HER2-positive breast cancer cell lines after anti-HER2 blockade, suggesting these roles in resistance to anti-HER2 therapy^{51,52}. These results suggest the potential use of phosphoproteomic analysis to explore acquired resistance upon treatment and to identify therapeutic kinase targets in clinical practice.

Genomic or transcriptomic comparisons of tumor with non-tumor adjacent tissue may help with patient stratification in clinical trials^{53,54}. In our study, kinases associated with the cell cycle (e.g., CDK2, CDK6) and the DNA damage response (e.g., ATM, ATR, CHEK2) were activated frequently in cancer, which is consistent with our previous research²³. These results suggest that phosphoproteomic analysis of paired tumor and non-tumor adjacent tissue may also be clinically useful for patient stratification and/or target identification.

The advent of next-generation sequencing paved the road to personalized medicine and has been associated with several clinical breakthroughs^{55,56}. Nonetheless, the majority of tumors lack 'driver' genetic alterations

that present clear therapeutic opportunities⁹. We propose that phosphoproteomic profiling combined with bioinformatic analysis may help to expand personalized cancer management by identifying targets at the post-translational level. Large-scale comprehensive studies in conjunction with genomic analysis will provide the basis for the development of clinical proteogenomic approaches and the potentiation of personalized medicine in oncology. Our study suggested large phosphoproteomic variety after drug therapy, representing diversity of molecular responses in individual tumors. Considering the broad overlapping of the quantified phosphosites and proteins in the cell lines and clinical samples, our data indicate that cell line mixture will be highly useful as a reference for clinical proteogenomic analysis.

The major limitation of this study is the small number of samples collected in a single institution. Large-scale studies are needed to confirm the utility of our methods not only for personalized medicine based on pre-treatment samples but also to identify the optimal therapeutic approach for addressing post-treatment changes in molecular dysregulation. Given the highly inter-individual variation in kinase activity after drug therapy, further oncological annotation is required for the selection of potential therapeutic kinases in the clinical setting. We mainly used phosphoproteomic data for the identification of biological features in this study. However, integrated approaches such as proteogenomic analyses will offer deeper insights into cancer biology and will ultimately expand therapeutic options. Improvements to microscaled-proteomic workflows using clinical specimens are needed to realize these analyses. Current hypotheses should be tested in preclinical models and then confirmed in clinical studies. Furthermore, the absolute level of phosphorylation varies in a site-specific manner. The biological implications of perturbations at each phosphosite are of interest; however, the roles of the majority of phosphosites are largely unknown. Thus, further research is required to understand the phosphorylation-dependent regulation of proteins, including HER2.

Our data demonstrated the feasibility of mass spectrometry-based phosphoproteomic analysis with small biopsy specimens to track phosphorylation status in clinically relevant pathways over a treatment course. It is expected that phosphoproteomic analysis can be applied to find not only optimal therapy based on the pre-treatment samples but also combination therapy by adding other drugs or switching to new therapy adapting to the post-treatment changes in molecular dysregulation. This new dynamic treatment strategy using phosphoproteomic analysis will contribute to disease control and prolongation of patient survival.

Conclusion

We show that highly sensitive phosphoproteomic analysis using endoscopic biopsy specimens is a clinically relevant tool for detecting dynamic molecular changes upon drug therapy. In addition, our data suggest that a phosphoproteomic analysis can be used to consecutively identify therapeutic targets in stage IV gastric cancer on an individual patient level.

Materials and methods

Clinical specimens. All patients were treated at the National Cancer Center Hospital (Tokyo, Japan). We collected endoscopic biopsy specimens from four patients with HER2-positive gastric cancer and four patients with HER2-negative gastric cancer. Post-treatment specimens from HER2-positive gastric cancer patients were obtained two months later after the initiation of drug therapy. In a single endoscopic procedure, three tumor specimens and three normal gastric mucosa specimens were collected concomitantly from each patient.

Each specimen was separately put in a screw-cap tube and immediately snap-frozen in liquid nitrogen within 20 s after collection. Frozen specimens were stored at -80 °C until further sample preparation.

All procedures involving human participants were performed in accordance with the ethical standards of the institutional and national research committee and with the Helsinki Declaration of 1964 and later versions. This study was approved by the Ethics Committees of the National Cancer Center Hospital (Tokyo, Japan) and National Institute of Biomedical Innovation Health and Nutrition (Osaka, Japan). Written informed consent was obtained from all patients. The date of protocol approval was 16 August 2017 at the National Cancer Center Hospital (Tokyo, Japan).

Homogenization and solubilization of patient specimens. Each frozen specimen was transferred to a 1.5 mL tube supplied for use with a PowerMasher 2 (Nippi, Tokyo, Japan) and mixed with phase transfer surfactant (PTS) buffer supplemented with cOmplete™ protease inhibitor and PhosStop™ phosphatase inhibitor⁵⁷. Each specimen was homogenized for 30 s, and subjected to boiling at 95 °C for 5 min. The cell lysates were further sonicated twice (15 min per set) with a Bioruptor sonicator (Cosmo Bio, Tokyo, Japan). The cell lysates were centrifuged at 20,000 rcf at 4 °C for 3 min and the supernatants of the corresponding three specimens were transferred to a new tube. After centrifugation, the protein concentration was measured with a detergent compatible (DC) protein assay kit.

Protein precipitation, digestion, and desalting of clinical specimens. To remove contaminants, 500 µg of protein in each cell lysate was precipitated with methanol/chloroform precipitation. The pellets were re-suspended in PTS buffer and processed using a modified protocol from a previous study^{23,57}. The amount of protein in the re-suspended solution was measured with a DC protein assay kit and 300 µg of each protein lysate was used for further steps. Then, the samples were reduced with tris (2-carboxyethyl) phosphine hydrochloride (TCEP) with a final concentration of 10 mM at 37 °C for 60 min, and alkylated with iodoacetamide (IAA) with a final concentration of 20 mM in the dark room at 37 °C for 30 min. Alkylation was terminated with L-cysteine with a final concentration of 21 mM at room temperature for 10 min. Each protein lysate was mixed with trypsin (protein weight: 1/50) and lysyl endopeptidase (protein weight: 1/50) and subjected to incubation for overnight at 37 °C. The samples were acidified with 1% trifluoroacetic acid (TFA) and centrifuged at 20,000 rcf for 10 min

at 4 °C. Supernatants were desalted and separated into two tubes (99% for phosphoproteomic analysis, 1% for global proteomic analysis)²³.

Enrichment of phosphopeptides in clinical specimens. Enrichment of phosphopeptides with Fe³⁺-immobilized metal affinity chromatography (IMAC) resin was performed^{23,58}. In this study, we enriched phosphopeptides on a stage-tip with Fe-IMAC resin. Briefly, a C¹⁸ disc was set in a 200- μ L disposable tip, and Fe-IMAC resin was set on the C¹⁸ disc. Desalted peptides were passed through the IMAC/C¹⁸ stage-tip. Phosphopeptides were eluted with 60% acetonitrile (ACN) plus 0.1% TFA, and purified on the lower C¹⁸ disc.

Preparation of cell line mixture as reference samples. MKN-28, MKN-45, MKN-74, NCI-N87, NUGC-3 and TMK-1 cells were cultured at 37 °C under 5% CO₂. These gastric cancer cell lines were maintained in Roswell Park Memorial Institute (RPMI)-1640 supplemented with 10% fetal bovine serum (FBS). The gastric cancer cells were harvested after washing with ice-cold phosphate buffered saline (PBS) buffer containing PhosSTOP (phosphatase inhibitor) and cOmplete (protease inhibitor). Pellets of the collected cells were quickly frozen in liquid nitrogen and stored at –80 °C prior to use. Lysis of the cell pellets was performed in PTS buffer supplemented with cOmplete protease inhibitor cocktail and PhosSTOP, and then all cell lysates were mixed. Protein concentration was determined using a DC protein assay according to the manufacturer's protocol. A total of 8 mg of protein lysate (four lysates with 2.0 mg proteins) was reduced, alkylated, desalted, and 99% of elution was subjected to enrichment of phosphopeptides for reference samples for phosphoproteomic analysis and 1% of elution was used for reference samples for global proteomic analysis⁵⁹.

Tandem mass tag (TMT) labeling and fractionation of peptides on C¹⁸/SCX stagetip. TMT labelling for each sample was conducted using TMT 10-plex isobaric label reagent according to the manufacturer's protocol²³. A correspondence table of each TMT label and each sample is summarized in Fig. S1. TMT-labelled peptides of each TMT batch were pooled and fractionated on a C¹⁸/SCX stage-tip⁶⁰.

LC–MS/MS analysis. LC–MS/MS was performed by coupling an UltiMate 3000 Nano LC system (Thermo Scientific, Bremen, Germany) and an HTC-PAL autosampler (CTC Analytics, Zwingen, Switzerland) to an Orbitrap Fusion Lumos mass spectrometer (Thermo Scientific)⁶¹. Peptides were delivered to an analytical column (75 μ m \times 30 cm, packed in-house with ReproSil-Pur C18-AQ, 1.9 μ m resin, Dr. Maisch, Ammerbuch, Germany) and separated at a flow rate of 280 nL/min using a 145-min gradient from 5 to 30% of solvent B (solvent A, 0.1% formic acid [FA]; solvent B, 0.1% FA and 99.9% ACN)⁶¹. The Orbitrap Fusion Lumos mass spectrometer was operated in the data-dependent mode⁶¹. For phosphoproteomic analysis, survey full scan MS spectra (m/z 375 to 1,500) were acquired in the Orbitrap with 120,000 resolution after accumulation of ions to a 4×10^5 target value⁶¹. Maximum injection time was set to 50 ms and dynamic exclusion was set to 30 s. MS2 analysis consisted of higher-energy collisional dissociation (HCD); automatic gain control (AGC) 1×10^5 ; normalized collision energy (NCE) 38; maximum injection time 105 ms; 50,000 resolution and isolation window of 0.7 Da⁶¹. For global proteome analysis, survey full scan MS spectra (m/z 375 to 1500) were acquired in the Orbitrap with 120,000 resolution after accumulation of ions to a 1×10^5 target value. Maximum injection time was set to 100 ms and dynamic exclusion was set to 10 s. MS2 analysis consisted of HCD; AGC 1×10^5 ; NCE 38; maximum injection time 315 ms; 120,000 resolution and isolation window of 0.7 Da.

Data processing for identification and quantification of peptides. The identification of proteins and phosphosites was carried out with MaxQuant 1.5.1.2 supported by the Andromeda search engine⁶². The reviewed amino acid database was obtained from the UniProt (human, release 2017_01) and combined with 262 common contaminants. Enzyme specificity was set to Trypsin/P (a C-terminal of Arg or Lys with the allowed cleavage at the proline bond). Miss-cleavages were tolerated up to two sites. Fixed modification was set as carbamidomethylation of cysteine residues. Methionine oxidation, serine, threonine, and tyrosine phosphorylation were assigned as variable modifications. False discovery rates of protein group, peptide-spectrum match (PSM), and posttranslational modification (PTM) site were less than 0.01. Peptides hit as “Reverse” or “Potential Contaminant” were not used in the following analysis. Only protein groups identified with at least two or more peptides (sum of razor and unique) were used in the further analysis. The cut-off criteria for localization probability at each phosphosite was greater than 0.75⁶³. Peptide-Spectrum Matches (PSMs) were summarized in Table S11 [for phosphoproteomic analysis] and Table S12 [for global proteomic analysis]).

Data processing for comparisons. Statistical analysis was carried out with Perseus 1.6.2.3⁶⁴. We adopted two methods of normalization for group comparisons and individual comparisons using the quantitative data of TMT reporter ion intensities with log₂ transformation. For the comparison of proteomic data between two different group (e.g., the pre-treatment HER2-positive gastric cancer group and the post-treatment HER2-positive gastric cancer group), the mean abundance value of a specific protein or phosphosite from the mixed cell line sample was subtracted from the corresponding value in each clinical sample and normalized by median centering of the values in each TMT channel. Next, batch correction was performed for TMT batches. In this study, proteins (or phosphosites) quantified at least one sample in each TMT batch (a total of four batches) were considered for subjects of imputation. Each minimum value was imputed to each protein (or phosphosite). Then, the batch effect was removed using the Combat function on sva package version 3.36.0. Using the corrected data, the mean quantitative value of protein (or phosphosite) of each group was calculated by averaging the quantitative values of clinical samples among the same group. Differentially expressed phosphosites with sig-

nificance between two groups were selected if a phosphosite had $\log_2 |\text{FC}| > 1$ with a $p < 0.05$ for the Welch test (comparisons between the pre-treatment HER2-positive T group and the HER2-negative T group) or a paired t -test (comparisons between the post-treatment HER2-positive T group and the pre-treatment HER2-positive T group) of a difference between two groups. Differentially expressed phosphosites with tendency between two groups were selected if a phosphosite had $\log_2 |\text{FC}| > 1$ with a $0.05 \leq p < 0.1$ for the Welch test or a paired t -test of a difference between two groups. For individual comparisons between paired post-treatment and pre-treatment HER2-positive gastric cancer, the quantitative phosphosite value of each clinical sample was normalized by median centering of the values in each TMT channel. Differentially expressed phosphosites were selected if a phosphosite had $\log_2 |\text{FC}| > 1$.

Principal component analysis (PCA). To understand whether there were differences between the clinical samples, PCA was performed using the `prcomp` function (R environment version 4.0.2). The visualization of PCA was performed by `ggplot2` package version 3.3.2.

Phosphorylation profiling in the ErbB signaling pathway. Molecular information on the ErbB pathway was downloaded from KEGG⁶⁵. \log_2 transformed fold change (FC) values of each phosphosite were manually plotted on the picture of the pathway.

Pathway enrichment analysis. Differentially expressed phosphosites with significance between two groups were subjected to the pathway analysis in WebGestalt using KEGG⁶⁶. Pathways with a p -value < 0.05 were selected as significant pathways.

Estimation of individual kinase activity. Kinase enrichment analysis on the ratio of quantitative values of phosphosites between two individual samples was performed using kinase-substrate enrichment analysis (KSEA)⁶⁷. We selected kinases that had more than one kinase-substrate relationship as registered in PhosphositePlus⁴¹. A p value of less than 0.05 indicated that a kinase was significantly dysregulated.

Received: 25 September 2021; Accepted: 8 March 2022

Published online: 25 March 2022

References

1. Ferlay, J. *et al.* GLOBOCAN 2012: Estimated cancer incidence, mortality and prevalence worldwide in 2012 v1.0. IARC CancerBase No. 11. In *International Agency for Research on Cancer* (2013).
2. Bang, Y. J. *et al.* Trastuzumab in combination with chemotherapy versus chemotherapy alone for treatment of HER2-positive advanced gastric or gastro-oesophageal junction cancer (ToGA): A phase 3, open-label, randomised controlled trial. *Lancet* **376**, 687–697 (2010).
3. Shitara, K. *et al.* Trastuzumab deruxtecan in previously treated HER2-positive gastric cancer. *N. Engl. J. Med.* **382**, 2419–2430 (2020).
4. Janjigian, Y. Y. *et al.* First-line nivolumab plus chemotherapy versus chemotherapy alone for advanced gastric, gastro-oesophageal junction, and oesophageal adenocarcinoma (CheckMate 649): A randomised, open-label, phase 3 trial. *Lancet* **398**, 27–40 (2021).
5. Kang, Y. K. *et al.* Nivolumab plus chemotherapy versus placebo plus chemotherapy in patients with HER2-negative, untreated, unresectable advanced or recurrent gastric or gastro-oesophageal junction cancer (ATTRACTION-4): A randomised, multicentre, double-blind, placebo-controlled, phase 3 trial. *Lancet Oncol.* **23**, 234–247 (2022).
6. The Cancer Genome Atlas Research Network. Comprehensive molecular characterization of gastric adenocarcinoma. *Nature* **513**, 202–209 (2014).
7. Cristescu, R. *et al.* Molecular analysis of gastric cancer identifies subtypes associated with distinct clinical outcomes. *Nat. Med.* **21**, 449–456 (2015).
8. Sunami, K. *et al.* The initial assessment of expert panel performance in core hospitals for cancer genomic medicine in Japan. *Int. J. Clin. Oncol.* **26**, 443–449 (2021).
9. Zehir, A. *et al.* Mutational landscape of metastatic cancer revealed from prospective clinical sequencing of 10,000 patients. *Nat. Med.* **23**, 703–713 (2017).
10. Yuki, S. *et al.* The nationwide cancer genome screening project in Japan SCRUM-Japan GI-SCREEN: Efficient identification of cancer genome alterations in advanced gastric cancer (GC) (American Society of Clinical Oncology, 2018).
11. Mertins, P. *et al.* Proteogenomics connects somatic mutations to signalling in breast cancer. *Nature* **534**, 55–62 (2016).
12. Zhang, B. *et al.* Proteogenomic characterization of human colon and rectal cancer. *Nature* **513**, 382–387 (2014).
13. Zhang, H. *et al.* Integrated proteogenomic characterization of human high-grade serous ovarian cancer. *Cell* **166**, 755–765 (2016).
14. Gillette, M. A. *et al.* Proteogenomic characterization reveals therapeutic vulnerabilities in lung adenocarcinoma. *Cell* **182**, 200–225.e235 (2020).
15. Wang, L. B. *et al.* Proteogenomic and metabolomic characterization of human glioblastoma. *Cancer Cell* **2021**(39), 509–528.e20 (2021).
16. Huang, C. *et al.* Proteogenomic insights into the biology and treatment of HPV-negative head and neck squamous cell carcinoma. *Cancer Cell* **39**, 361–379.e316 (2021).
17. Petralia, F. *et al.* Integrated proteogenomic characterization across major histological types of pediatric brain cancer. *Cell* **183**, 1962–1985.e1931 (2020).
18. Clark, D. J. *et al.* Integrated proteogenomic characterization of clear cell renal cell carcinoma. *Cell* **179**, 964–983.e931 (2019).
19. Krug, K. *et al.* Proteogenomic landscape of breast cancer tumorigenesis and targeted therapy. *Cell* **183**, 1436–1456.e1431 (2020).
20. Khorsandi, S. E. *et al.* Computational analysis of cholangiocarcinoma phosphoproteomes identifies patient-specific drug targets. *Cancer Res.* **81**, 5765–5776 (2021).
21. Martín-Guerrero, S. M. *et al.* PARP-1 activation after oxidative insult promotes energy stress-dependent phosphorylation of YAP1 and reduces cell viability. *Biochem. J.* **477**, 4491–4513 (2020).

22. Mertins, P. *et al.* Ischemia in tumors induces early and sustained phosphorylation changes in stress kinase pathways but does not affect global protein levels. *Mol. Cell. Proteomics*. **13**, 1690–1704 (2014).
23. Abe, Y. *et al.* Comprehensive characterization of the phosphoproteome of gastric cancer from endoscopic biopsy specimens. *Theranostics*. **10**, 2115–2129 (2020).
24. Zhang, X. *et al.* Mechanistic insight into Myc stabilization in breast cancer involving aberrant Axin1 expression. *Proc. Natl. Acad. Sci. U. S. A.* **109**, 2790–2795 (2012).
25. Park, K., Kwak, K., Kim, J., Lim, S. & Han, S. c-myc amplification is associated with HER2 amplification and closely linked with cell proliferation in tissue microarray of nonselected breast cancers. *Hum. Pathol.* **36**, 634–639 (2005).
26. Imami, K. *et al.* Temporal profiling of lapatinib-suppressed phosphorylation signals in EGFR/HER2 pathways. *Mol. Cell. Proteom.* **11**, 1741–1757 (2012).
27. Urisman, A. *et al.* Targeted phosphoproteomics of the Ras signaling network reveal regulatory mechanisms mediated by oncogenic KRAS. *bioRxiv* **69**, 5460 (2019).
28. Zhou, C. *et al.* Difference of molecular alterations in HER2-positive and HER2-negative gastric cancers by whole-genome sequencing analysis. *Cancer Manag. Res.* **10**, 3945–3954 (2018).
29. Ito, M. *et al.* Targeting PKC α -PAK1 signaling pathways in EGFR and KRAS mutant adenocarcinoma and lung squamous cell carcinoma. *Cell Commun. Signal.* **17**, 137 (2019).
30. Li, T. *et al.* P21-activated protein kinase (PAK2)-mediated c-Jun phosphorylation at 5 threonine sites promotes cell transformation. *Carcinogenesis* **32**, 659–666 (2011).
31. Molli, P. R., Li, D. Q., Murray, B. W., Rayala, S. K. & Kumar, R. PAK signaling in oncogenesis. *Oncogene* **28**, 2545–2555 (2009).
32. Chang, Y., Park, K. H., Lee, J. E. & Han, K. C. Phosphoproteomic analysis reveals PAK2 as a therapeutic target for lapatinib resistance in HER2-positive breast cancer cells. *Biochem. Biophys. Res. Commun.* **505**, 187–193 (2018).
33. Arias-Romero, L. E. *et al.* A Rac-Pak signaling pathway is essential for ErbB2-mediated transformation of human breast epithelial cancer cells. *Oncogene* **29**, 5839–5849 (2010).
34. Guo, Y. J. *et al.* ERK/MAPK signalling pathway and tumorigenesis. *Exp. Ther. Med.* **19**, 1997–2007 (2020).
35. Martin, K. A., Schalm, S. S., Romanelli, A., Keon, K. L. & Blenis, J. Ribosomal S6 kinase 2 inhibition by a potent C-terminal repressor domain is relieved by mitogen-activated protein-extracellular signal-regulated kinase kinase-regulated phosphorylation. *J. Biol. Chem.* **276**, 7892–7898 (2001).
36. Nateri, A. S., Spencer-Dene, B. & Behrens, A. Interaction of phosphorylated c-Jun with TCF4 regulates intestinal cancer development. *Nature* **437**, 281–285 (2005).
37. Adhikary, S. & Eilers, M. Transcriptional regulation and transformation by Myc proteins. *Nat. Rev. Mol. Cell Biol.* **6**, 635–645 (2005).
38. Zeng, F. *et al.* Identification of key pathways and genes in response to trastuzumab treatment in breast cancer using bioinformatics analysis. *Oncotarget* **9**, 32149–32160 (2018).
39. Pellarin, I., Belletti, B. & Baldassarre, G. RNA splicing alteration in the response to platinum chemotherapy in ovarian cancer: A possible biomarker and therapeutic target. *Med. Res. Rev.* **41**, 586–615 (2021).
40. Martin, L. P., Hamilton, T. C. & Schilder, R. J. Platinum resistance: The role of DNA repair pathways. *Clin. Cancer Res.* **14**, 1291–1295 (2008).
41. Hornbeck, P. V. *et al.* PhosphoSitePlus: A comprehensive resource for investigating the structure and function of experimentally determined post-translational modifications in man and mouse. *Nucleic Acids Res.* **40**, D261–D270 (2012).
42. Won, S. Y., Park, J. J., Shin, E. Y. & Kim, E. G. PAK4 signaling in health and disease: Defining the PAK4-CREB axis. *Exp. Mol. Med.* **51**, 1–9 (2019).
43. Weaver, A. M. & Silva, C. M. Signal transducer and activator of transcription 5b: A new target of breast tumor kinase/protein tyrosine kinase 6. *Breast Cancer Res.* **9**, R79 (2007).
44. Vu, T. & Claret, F. X. Trastuzumab: Updated mechanisms of action and resistance in breast cancer. *Front. Oncol.* **2**, 62 (2012).
45. Tomioka, H. *et al.* Inhibition of the mTOR/S6K signal is necessary to enhance fluorouracil-induced apoptosis in gastric cancer cells with HER2 amplification. *Int. J. Oncol.* **41**, 551–558 (2012).
46. Kataoka, Y. *et al.* Association between gain-of-function mutations in PIK3CA and resistance to HER2-targeted agents in HER2-amplified breast cancer cell lines. *Ann. Oncol.* **21**, 255–262 (2010).
47. Ren, W. *et al.* mTORC1 signaling and IL-17 expression: Defining pathways and possible therapeutic targets. *Eur. J. Immunol.* **46**, 291–299 (2016).
48. Gschwantler-Kaulich, D. *et al.* HER specific TKIs exert their antineoplastic effects on breast cancer cell lines through the involvement of STAT5 and JNK. *PLoS One*. **11**, e0146311 (2016).
49. Diab, S., Yu, M. & Wang, S. CDK7 inhibitors in cancer therapy: The sweet smell of success? *J. Med. Chem.* **63**, 7458–7474 (2020).
50. Wang, Q. *et al.* Upregulation of CDK7 in gastric cancer cell promotes tumor cell proliferation and predicts poor prognosis. *Exp. Mol. Pathol.* **100**, 514–521 (2016).
51. Stuhlmiller, T. J. *et al.* Inhibition of lapatinib-induced kinome reprogramming in ERBB2-positive breast cancer by targeting BET family bromodomains. *Cell Rep.* **11**, 390–404 (2015).
52. Li, G. *et al.* Mechanisms of acquired resistance to trastuzumab emtansine in breast cancer cells. *Mol. Cancer Ther.* **17**, 1441–1453 (2018).
53. Rodon, J. *et al.* Genomic and transcriptomic profiling expands precision cancer medicine: The WINTHER trial. *Nat. Med.* **25**, 751–758 (2019).
54. Sunami, K. *et al.* Feasibility and utility of a panel testing for 114 cancer-associated genes in a clinical setting: A hospital-based study. *Cancer Sci.* **110**, 1480–1490 (2019).
55. Kwak, E. L. *et al.* Anaplastic lymphoma kinase inhibition in non-small-cell lung cancer. *N. Engl. J. Med.* **363**, 1693–1703 (2010).
56. Drilon, A. *et al.* Efficacy of larotrectinib in TRK fusion-positive cancers in adults and children. *N. Engl. J. Med.* **378**, 731–739 (2018).
57. Masuda, T., Tomita, M. & Ishihama, Y. Phase transfer surfactant-aided trypsin digestion for membrane proteome analysis. *J. Proteome Res.* **7**, 731–740 (2008).
58. Matsumoto, M. *et al.* Large-scale proteomic analysis of tyrosine-phosphorylation induced by T-cell receptor or B-cell receptor activation reveals new signaling pathways. *Proteomics* **9**, 3549–3563 (2009).
59. Abe, Y. *et al.* Deep phospho- and phosphotyrosine proteomics identified active kinases and phosphorylation networks in colorectal cancer cell lines resistant to cetuximab. *Sci. Rep.* **7**, 10463 (2017).
60. Adachi, J. *et al.* Improved proteome and phosphoproteome analysis on a cation exchanger by a combined acid and salt gradient. *Anal. Chem.* **88**, 7899–7903 (2016).
61. Mizuta, H. *et al.* Gilteritinib overcomes lorlatinib resistance in ALK-rearranged cancer. *Nat. Commun.* **12**, 1261 (2021).
62. Cox, J. & Mann, M. MaxQuant enables high peptide identification rates, individualized p.p.b.-range mass accuracies and proteome-wide protein quantification. *Nat. Biotechnol.* **26**, 1367–1372 (2008).
63. Sharma, K. *et al.* Ultra-deep human phosphoproteome reveals a distinct regulatory nature of Tyr and Ser/Thr-based signaling. *Cell Rep.* **8**, 1583–1594 (2014).
64. Tyanova, S. *et al.* The Perseus computational platform for comprehensive analysis of (prote)omics data. *Nat. Methods*. **13**, 731–740 (2016).
65. Kanehisa, M. & Goto, S. KEGG: Kyoto encyclopedia of genes and genomes. *Nucleic Acids Res.* **28**, 27–30 (2000).

66. Wang, J., Vasaikar, S., Shi, Z., Greer, M. & Zhang, B. WebGestalt 2017: A more comprehensive, powerful, flexible and interactive gene set enrichment analysis toolkit. *Nucleic Acids Res.* **45**, W130-w137 (2017).
67. Wiredja, D. D., Koyutürk, M. & Chance, M. R. The KSEA App: A web-based tool for kinase activity inference from quantitative phosphoproteomics. *Bioinformatics* **33**, 3489–3491 (2017).

Acknowledgements

We thank A. Murooka for assistance with obtaining clinical specimens.

Author contributions

Conceptualization, H.H., Y.A., H.S., N.B., T.T., and J.A.; methodology, H.H., Y.A., T.T., and J.A.; software, J.I., T.T., and J.A.; formal analysis, H.H., and Y.N.; investigation, H.H., Y.A., Y.N., H.S., N.B., K.H., T.T., and J.A.; resources, M.A., H.S., and N.B.; data curation, H.H., and Y.N.; writing—original draft preparation, H.H., Y.A. and Y.N.; writing—review and editing, K.H., H.S., N.B., T.T., and J.A.; visualization, H.H., and Y.N.; supervision, N.B., K.M., T.T., and J.A.; project administration, H.S., N.B., T.T., and J.A.; funding acquisition, H.H., and J.A. All authors have read and agreed to the published version of the manuscript.

Funding

This work was supported by AMED under Grant Number JP19ck0106465h0001 awarded to H.S., N.B., K.H., T.T., and J.A. and JSPS KAKENHI Grant Number 20K17069 awarded to H.H.

Competing interests

The authors declare no competing interests.

Additional information

Supplementary Information The online version contains supplementary material available at <https://doi.org/10.1038/s41598-022-08430-7>.

Correspondence and requests for materials should be addressed to T.T. or J.A.

Reprints and permissions information is available at www.nature.com/reprints.

Publisher's note Springer Nature remains neutral with regard to jurisdictional claims in published maps and institutional affiliations.



Open Access This article is licensed under a Creative Commons Attribution 4.0 International License, which permits use, sharing, adaptation, distribution and reproduction in any medium or format, as long as you give appropriate credit to the original author(s) and the source, provide a link to the Creative Commons licence, and indicate if changes were made. The images or other third party material in this article are included in the article's Creative Commons licence, unless indicated otherwise in a credit line to the material. If material is not included in the article's Creative Commons licence and your intended use is not permitted by statutory regulation or exceeds the permitted use, you will need to obtain permission directly from the copyright holder. To view a copy of this licence, visit <http://creativecommons.org/licenses/by/4.0/>.

© The Author(s) 2022